Activation cross sections of alpha-particle-induced reactions on natural tungsten for osmium and rhenium radionuclides

Naoyuki Ukon [a], Masayuki Aikawa [b,c,d,*], Moemi Saito [d], Masayuki Hagiwara [e], Hiroshi Yashima [f], Yukiko Komori [g], Hiromitsu Haba [g], Sándor Takács [h], Ferenc Ditrói [h], Zoltán Szűcs [h]

[a] *Advanced Clinical Research Center, Fukushima Medical University, Fukushima 960-1295, Japan*

[b] *Faculty of Science, Hokkaido University, Sapporo 060-0810, Japan*

[c] *Global Center for Biomedical Science and Engineering, Faculty of Medicine, Hokkaido University, Sapporo 060-8648, Japan*

[d] *Graduate School of Biomedical Science and Engineering, Hokkaido University, Sapporo 060-8638, Japan*

[e] *National Institutes for Quantum Science and Technology, Sendai 984-8579, Japan*

[f] *Institute for Integrated Radiation and Nuclear Science, Kyoto University, Kumatori 590-0494, Japan*

[g] *Nishina Center for Accelerator-Based Science, RIKEN, Wako 351-0198, Japan*

[h] *Institute for Nuclear Research, (ATOMKI), 4026 Debrecen, Hungary*

Abstract

We measured activation cross sections of alpha-particle-induced reactions on natural tungsten targets. The stacked-foil activation technique and gamma-ray spectrometry were used. Production cross sections of ^{185,183m,183g,182g}Os and ^{188g,186g,184g,183g,182g,181}Re were determined. The results were compared with experimental literature data and the TENDL-2019 and TENDL-2021 values. The cross sections of the most reactions were determined for the first time.

Keyword

Rhenium-186,188; Tungsten target; alpha-particle irradiation; Cross section; Excitation function

1. Introduction

Rhenium radioisotopes can be used for nuclear medicine [1–3]. ^{186g}Re with a half-life of 3.7 d decays with emission of beta particles and gamma rays. The maximum energy of the beta particles is 1.07 MeV, which enables the beta particles to pass through the average range of 1.1 mm in soft tissue and 0.5 mm in bone [1]. ^{188g}Re is also a beta emitter. It has a half-life of 17 h and decays with emission of a higher-energy beta particle (2.12 MeV at maximum) and gamma rays. The decay properties enable us to apply the radionuclide to a variety of medical applications [3]. Both rhenium radionuclides can be used for theranostics, the combination of therapy and diagnosis.

[*] Corresponding author: Masayuki AIKAWA (aikawa@sci.hokudai.ac.jp), Faculty of Science, Hokkaido University, Sapporo 060-0810, Japan

These radionuclides can be produced by charged-particle-induced reactions on tungsten. Among possible reactions, we focused on alpha-particle-induced reactions on tungsten due to the shortage of experimental data. In a literature survey using the EXFOR library [4] and Nuclear Science References (NSR) [5], we found two experimental studies for cross sections using ^{186}W enriched targets [6,7]. However, the cross sections were largely different from each other. Therefore, additional measurements were required for reliable cross sections.

Accordingly we performed an experiment to measure activation cross sections of alpha-particle-induced reactions on a natural tungsten target, which consists of five isotopes, ^{180}W (0.12%), ^{182}W (26.50%), ^{183}W (14.31%), ^{184}W (30.64%), and ^{186}W (28.43%) [8]. Production cross sections of ^{185,183m,183g,182g}Os and ^{188g,186g,184g,183g,182g,181}Re were determined. The usage of isotopically enriched targets is expected to avoid or reduce the production of impurities. The measured cross sections are expected to contribute to search for the best production routes of these radionuclides.

2. Experimental

In this experiment a 50-MeV alpha-particle beam at the RIKEN AVF cyclotron was used to irradiate the stacked-foil target. We adopted well-established experimental methods, stacked-foil activation technique and off-line high-resolution gamma-ray spectrometry.

The stacked target consisted of thin and pure metallic foils of natural tungsten (^{nat}W) and titanium (^{nat}Ti). The ^{nat}W (0.015×25×50 mm, 99.95% purity) and ^{nat}Ti (0.005×50×100 mm, 99.6% purity) foils were purchased from Nilaco Corp., Japan. The ^{nat}Ti foil was used for the $^{nat}Ti(\alpha,x)^{51}Cr$ monitor reaction to assess beam parameters and target thicknesses. The lateral size and weight of the purchased foils were measured and average thicknesses of the foils were deduced. The measured average thicknesses of the ^{nat}W and ^{nat}Ti foils were 30.0 and 2.30 mg/cm^2, respectively. The foils were cut into 8×8 mm pieces to fit a target holder serving as a Faraday cup. Fourteen sets of the W-Ti-Ti foils were stacked in the target holder. The first ^{nat}Ti foil in each W-Ti-Ti set was used as a catcher foil of recoiled products from the ^{nat}W foil. The second ^{nat}Ti foils were used for the monitor reaction under assumption that the recoiled products from the second foils were compensated by the recoils from the first foils.

The stacked target was irradiated for 60 min with an alpha-particle beam collimated to a 3-mm diameter. The average beam intensity measured by the Faraday cup was 189 nA. The primary beam energy determined by the time-of-flight method [8] was 50.7±0.2 MeV. The energy degradation in the stacked target was calculated using stopping powers obtained from the SRIM code [8].

The high-resolution gamma-ray spectrometry was performed using two high-purity germanium detectors (ORTEC GEM30P4-70) and analysis software (SEIKO EG&G Gamma Studio). The efficiency of the detectors was calibrated using a gamma-ray point source consisting of $^{57,60}Co$, ^{85}Sr, ^{88}Y, ^{109}Cd, ^{113}Sn, ^{137}Cs, ^{139}Ce, ^{203}Hg, and ^{241}Am (Eckert & Ziegler Isotope Products). Spectra of each irradiated ^{nat}W foil together with the following ^{nat}Ti catcher foil were measured three times (Ser. 1-3) with different cooling time from 21 h to 4.8 d, respectively. The associated dead time was less than 6.9%. The experimental parameters were summarized in Table 1. Nuclear data were retrieved from the online databases, NuDat 3.0 [9], LiveChart [10], Lund/LBNL Nuclear Data Search [11] and QCalc [12]. The retrieved data are summarized in Table 2.

Low energy gamma rays generated in the target foils were partly absorbed by the target foil themselves. The measured activity was required to correct using the following formula [13]

$$A(E) = A_0(E)\frac{\rho[\mu(E)/\rho]d}{1-\exp\left[-\rho(\mu(E)/\rho)d\right]} \tag{1}$$

where $A_0(E)$ is the measured activity (s^{-1}) for the gamma ray at the energy E, $A(E)$ is the corrected activity (s^{-1}), d is the thickness (cm), ρ is the density of the foil (g cm^{-3}), $\mu(E)/\rho$ is the mass attenuation coefficient (cm^2 g^{-1}) at the energy E interpolated using values retrieved from the online database [14].

Activation cross sections were deduced using the following formula

$$\sigma = \frac{N_\gamma \lambda}{\varepsilon_d \varepsilon_\gamma \varepsilon_t N_t N_b (1-e^{-\lambda t_b}) e^{-\lambda t_c} (1-e^{-\lambda t_m})} \tag{2}$$

where N_γ is the net count of the photopeak area, λ is the decay constant (s^{-1}), ε_d is the detector efficiency,

ε_γ is the gamma-ray intensity, ε_t is the dead time correction, N_t is the surface density of target atoms (cm^{-2}), N_b is the number of projectiles per unit time (s^{-1}), t_b is the irradiation time (s), t_c is the cooling time (s), and t_m is the acquisition time (s). The measured net count N_γ of the low energy gamma rays was corrected using Eq. (1).

Cross sections of the ^{nat}Ti(α,x)^{51}Cr monitor reaction were derived to assess the beam parameters and target thicknesses. Each second ^{nat}Ti foil of the Ti-Ti pairs was used to deduce the cross sections of the monitor reaction. The cross sections were derived from measured net counts of the gamma line at 320.08 keV (I_γ = 9.91%). The derived cross sections are shown in Fig. 1 with the recommended values of International Atomic Energy Agency (IAEA) [15,16]. We found a good agreement with the recommended values. The measured beam parameters and target thicknesses were adopted without any correction for cross section deduction.

Table 1. Experimental parameters.

Target	
W	30.0 mg/cm^2
Ti	2.30 mg/cm^2
Configuration	14 sets of W-Ti-Ti foils
Beam	
Energy	50.7 ±0.2 MeV
Average intensity	189 ±9 nA
Irradiation period	60 min
Measurement (cooling and measuring time, distance, and dead time in each series)	
Ser. 1	21-33 h, 1.0-11 h, 5-50 cm, 0.2-6.9%
Ser. 2	46-72 h, 1.0-9.7 h, 2-30 cm, 0.3-6.0%
Ser. 3	3.0-4.8 d, 2.0-11 h, 2-20 cm, <3.7%

Table 2. Reaction and decay data of reaction products [9–12].

Nuclide	Half-life	Decay mode (%)	E_γ (keV)	I_γ (%)	Contributing reaction	Q-value (MeV)
^{185}Os	93.6 d	ε (100)	**646.116**	78(3)	^{182}W(α,n)	-11.1
					^{183}W(α,2n)	-17.3
					^{184}W(α,3n)	-24.7
					^{186}W(α,5n)	-37.6
^{183m}Os	9.9 h	ε+β$^+$ (85)	1101.93	49.2(13)	^{180}W(α,n)	-11.8
		IT (15)	**1107.93**	22.5(6)	^{182}W(α,3n)	-26.5
					^{183}W(α,4n)	-32.7
					^{184}W(α,5n)	-40.1
^{183g}Os	13.0 h	ε+β$^+$ (100)	114.43	21.1(3)	^{180}W(α,n)	-11.6

			381.74	91.6(15)	$^{182}W(\alpha,3n)$	-26.4
					$^{183}W(\alpha,4n)$	-32.6
					$^{184}W(\alpha,5n)$	-40.0
^{182g}Os	21.84 h	ε (100)	**130.80**	3.30(17)	$^{180}W(\alpha,2n)$	-18.4
			180.20	34.1(22)	$^{182}W(\alpha,4n)$	-33.5
			263.29	6.76(25)	$^{183}W(\alpha,5n)$	-39.7
			510.04	52.4(10)	$^{184}W(\alpha,6n)$	-47.1
^{188g}Re	17.003 h	β^- (100)	**155.044**	15.49(6)	$^{186}W(\alpha,d)$	-14.2
					^{188}W decay	
^{186g}Re	3.7186 d	β^- (92.53)	**137.157**	9.47(3)	$^{183}W(\alpha,p)$	-9.3
		ε (7.47)			$^{184}W(\alpha,d)$	-14.5
					$^{186}W(\alpha,tn)$	-21.2
^{184g}Re	35.4 d	$\varepsilon+\beta^+$ (100)	111.2174	17.2(7)	$^{182}W(\alpha,d)$	-14.7
			792.067	37.7(11)	$^{183}W(\alpha,t)$	-14.7
			894.760	15.7(5)	$^{184}W(\alpha,tn)$	-22.1
			903.282	38.1(12)	$^{186}W(\alpha,t3n)$	-35.0
^{183g}Re	70.0 d	ε (100)	**162.330**	25.1(22)	$^{180}W(\alpha,p)$	-8.7
					$^{182}W(\alpha,t)$	-15.0
					$^{183}W(\alpha,tn)$	-21.2
					$^{184}W(\alpha,t2n)$	-28.6
					$^{186}W(\alpha,t4n)$	-41.5
					^{183}Os decay	
^{182g}Re	64.2 h	$\varepsilon+\beta^+$ (100)	100.10	16.5(6)	$^{180}W(\alpha,d)$	-14.9
			169.15	11.4(8)	$^{182}W(\alpha,tn)$	-23.4
			229.32	25.8(7)	$^{183}W(\alpha,t2n)$	-29.6
			351.07	10.3(8)	$^{184}W(\alpha,t3n)$	-37.0
			1076.2	10.6(4)		
			1121.3	22.1(9)		
			1221.4	17.5(6)		
			1231.0	14.9(5)		
			1427.3	9.8(3)		
^{181}Re	19.9 h	$\varepsilon+\beta^+$ (100)	360.7	20(4)	$^{180}W(\alpha,t)$	-15.6
			365.5	56(7)	$^{182}W(\alpha,t2n)$	-30.4
					$^{183}W(\alpha,t3n)$	-36.6
					$^{184}W(\alpha,t4n)$	-44.0
					^{181}Os decay	
^{51}Cr	27.7025 d	ε (100)	**320.0824**	9.91(10)	$^{nat}Ti(\alpha,x)^{51}Cr$	

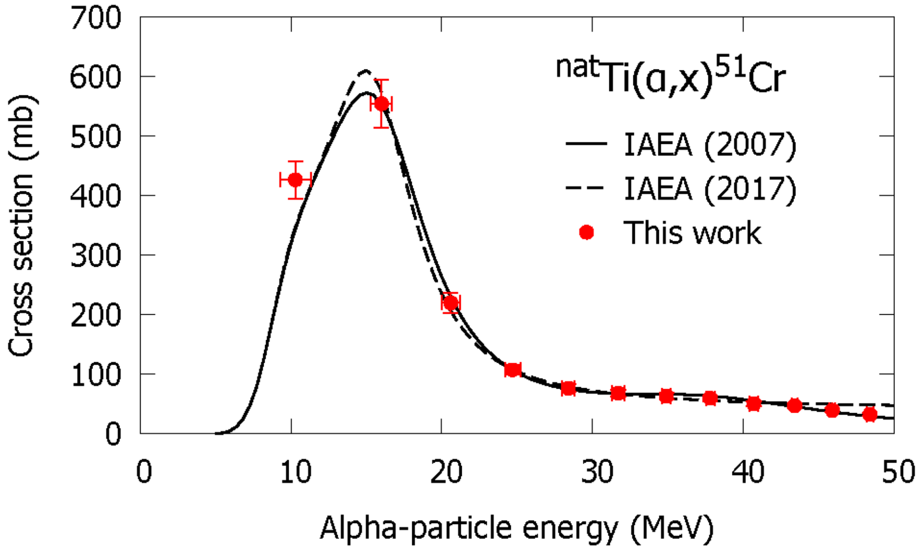

Fig. 1. Excitation function of the $^{nat}Ti(\alpha,x)^{51}Cr$ monitor reaction in comparison with the IAEA recommended values [15,16].

3. Results and discussion

Activation cross sections of alpha-particle-induced reactions on natural tungsten were measured. The cross sections for production of $^{185,183m,183g,182}Os$ and $^{188g,186g,184g,183g,182g,181}Re$ were determined. The derived cross sections are numerically tabulated in Tables 3 and 4 and graphically shown in Figs. 2-11 with experimental data published earlier [6,7] and theoretically calculated values in TENDL-2019 and TENDL-2021 [17]. Only the TENDL-2019 values are shown if independent cross sections for a ground or excited state are required, since these are not always explicitly mentioned in the corresponding TENDL-2021 library files for all the cases under study. The total uncertainty of the projectile energy was propagated from the uncertainties of the primary beam energy (±0.2 MeV) and target thicknesses (1%). The total energy loss in each ^{nat}W foil is also listed in the first column in parenthesis.

The total uncertainties of the cross sections (7.4–26.5%) are calculated from the square roots of the quadratic summation of each component; beam intensity (5%), gamma-ray intensity (0.3–12.5%), detector efficiency (5%), target thickness (1%) and counting statistics (0.2–22.3%).

Table 3. Production cross sections of osmium radioisotopes.

Energy (MeV)	^{185}Os (mb)	^{183m}Os (mb)	^{183g}Os (mb)	$^{182g}Os^{(cum)}$ (mb)
49.7 ±0.2 (1.9)	308 ±25	34.3 ±3.3	344 ±26	428 ±39
47.3 ±0.2 (2.0)	215 ±18	28.3 ±2.6	297 ±22	348 ±31
44.8 ±0.2 (2.1)	188 ±16	33.5 ±2.9	334 ±25	266 ±24
42.1 ±0.2 (2.2)	219 ±18	38.5 ±3.2	342 ±26	131 ±13
39.4 ±0.3 (2.3)	326 ±27	42.6 ±3.4	337 ±26	35.6 ±4.2
36.5 ±0.3 (2.4)	404 ±33	41.3 ±3.4	281 ±21	
33.5 ±0.3 (2.5)	386 ±32	33.4 ±2.7	191 ±15	
30.2 ±0.4 (2.7)	298 ±24	13.4 ±1.2	66.9 ±5.2	
26.7 ±0.4 (2.9)	153 ±13		1.25 ±0.11	
22.9 ±0.5 (3.2)	92.8 ±7.6		0.160 ±0.014	
18.6 ±0.6 (3.6)	24.0 ±2.0		0.0740 ±0.0056	
13.5 ±0.8 (4.4)	0.0999 ±0.0099			

Table 4. Production cross sections of rhenium radioisotopes.

Energy (MeV)	^{188g}Re (mb)	^{186g}Re (mb)	^{184g}Re (mb)	$^{183g}Re^{(cum)}$ (mb)	^{182g}Re (mb)	$^{181}Re^{(cum)}$ (mb)
49.7 ±0.2 (1.9)		11.1 ±1.2	18.8 ±2.1	424 ±48	6.88 ±0.76	21.8 ±3.2
47.3 ±0.2 (2.0)		7.42 ±0.95	17.2 ±2.1	372 ±42	2.94 ±0.45	3.55 ±0.63
44.8 ±0.2 (2.1)		7.43 ±0.97	15.2 ±1.9	401 ±46	1.46 ±0.33	1.93 ±0.43
42.1 ±0.2 (2.2)		6.10 ±0.73	11.7 ±1.4	414 ±47		1.76 ±0.37
39.4 ±0.3 (2.3)		6.15 ±0.50	10.0 ±0.9	406 ±46		2.00 ±0.35
36.5 ±0.3 (2.4)		5.69 ±0.45	7.72 ±0.67	341 ±39		1.51 ±0.32

33.5 ±0.3 (2.5)		4.17 ±0.36	5.11 ±0.47	238 ±27		0.719 ±0.191
30.2 ±0.4 (2.7)	3.07 ±0.49	2.51 ±0.23	2.75 ±0.30	85.1 ±9.7		
26.7 ±0.4 (2.9)	0.843 ±0.113	0.980 ±0.075	0.950 ±0.098	1.77 ±0.23		
22.9 ±0.5 (3.2)		0.132 ±0.019				

3.1 The $^{nat}W(\alpha,xn)^{185}Os$ reaction

The production cross sections of ^{185}Os ($T_{1/2}$ = 93.6 d) were determined using the interference-free gamma line at 646.116 keV (I_γ = 78%). The spectra measured in Ser. 3 were used for the cross section deduction. The derived cross sections are shown in Fig. 2 in comparison with theoretical prediction in TENDL-2019 and TENDL-2021. The peak position of TENDL-2021 [17] at 35 MeV composed of the dominant contribution of the $^{184}W(\alpha,3n)^{185}Os$ reaction is consistent with our result. The agreement with the TENDL-2021 values is better than that with the TENDL-2019 values. No experimental data were found in the literature survey.

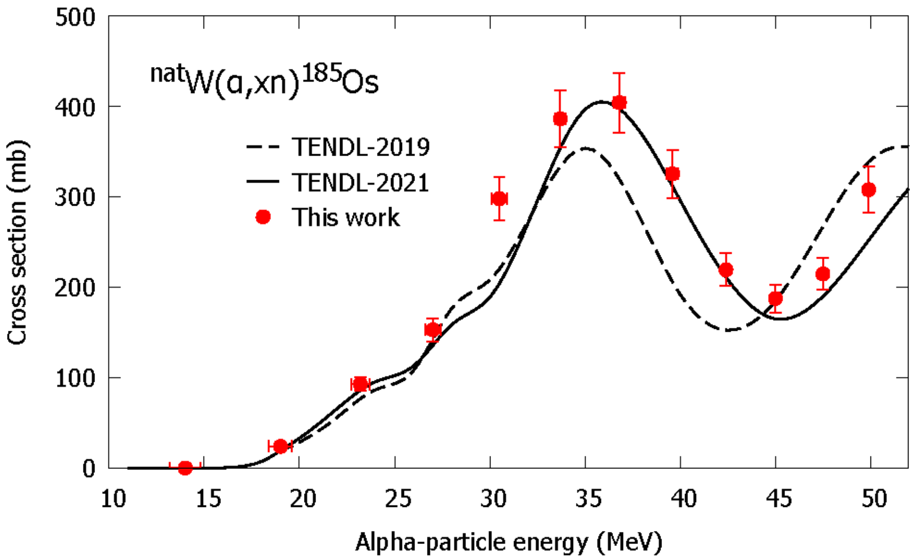

Fig. 2. Cross sections of the $^{nat}W(\alpha,xn)^{185}Os$ reaction with the TENDL-2019 and TENDL-2021 values [17].

3.2 The $^{nat}W(\alpha,xn)^{183m}Os$ reaction

Osmium-183 has two metastable states, the ground state ^{183g}Os ($T_{1/2}$ = 13.0 h) and the excited state ^{183m}Os at 0.171 MeV ($T_{1/2}$ = 9.9 h). The production cross sections of ^{183m}Os were determined using the interference-free gamma line at 1107.93 keV (I_γ = 22.5%) measured in Ser. 1. The more intense gamma line at 1101.93 keV (I_γ = 49.2%) was not selected because the contribution of the 1103.5-keV gamma line (I_γ = 0.69%) from ^{181}Re ($T_{1/2}$ = 19.9 h) could be included.

The result is shown in Fig. 3 with theoretical prediction of TENDL-2019 [17]. The TENDL-2019 data are different both in shape and in amplitude from our experimental data. No experimental data were found in the literature survey.

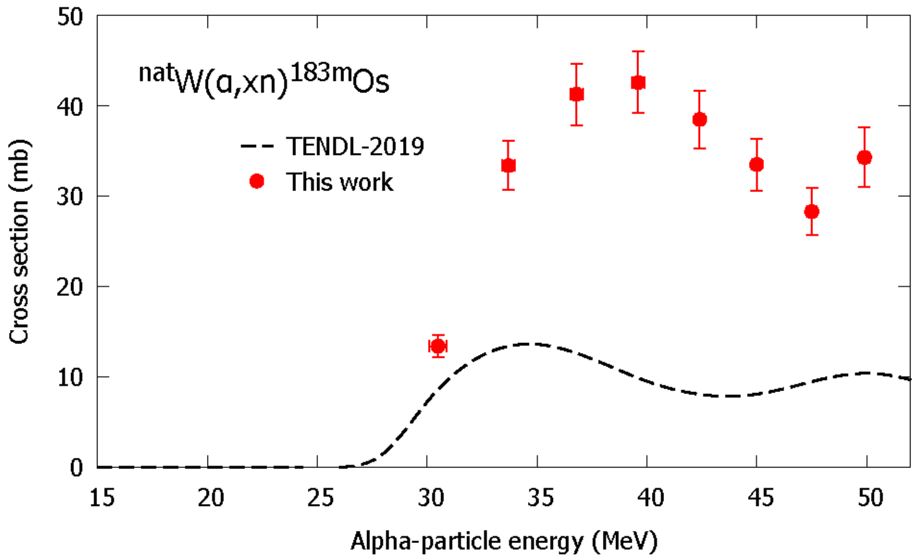

Fig. 3. Cross sections of the $^{nat}W(\alpha,xn)^{183m}Os$ reaction with the TENDL-2019 values [17].

3.3 The $^{nat}W(\alpha,xn)^{183g}Os$ reaction

The intense gamma line at 381.74 keV (I_γ = 91.6%) of the spectra in Ser. 1 was used to derive production cross sections of ^{183g}Os ($T_{1/2}$ = 13.0 h). The gamma line could include possible contribution of weak gamma lines from co-produced rhenium isotopes, such as 380.34 keV (I_γ = 0.0046%) from ^{184}Re ($T_{1/2}$ = 35.4 d), 381.82 keV (I_γ = 0.063%) from ^{184m}Re ($T_{1/2}$ = 169 d), and 382.3 keV (I_γ = 0.27%) from ^{181}Re ($T_{1/2}$ = 19.9 h). These weak gamma lines were found to be negligible in the adopted spectra because other intense gamma lines were missing. The co-produced isomer ^{183m}Os ($T_{1/2}$ = 9.9 h) partly decayed to ^{183g}Os (IT: 15%) and to ^{183}Re ($\varepsilon+\beta^+$: 85%) during the cooling time. The partial contribution of ^{183m}Os to ^{183g}Os was estimated using the cross sections determined in section 3.2 and subtracted.

The independent cross sections are shown in Fig. 4 with theoretical prediction in TENDL-2019 [17]. The TENDL-2019 data are slightly different from our data although the peak composed mainly of the $^{182}W(\alpha,3n)^{183g}Os$ reaction at around 40 MeV is consistent. There are no experimental data found in the literature survey.

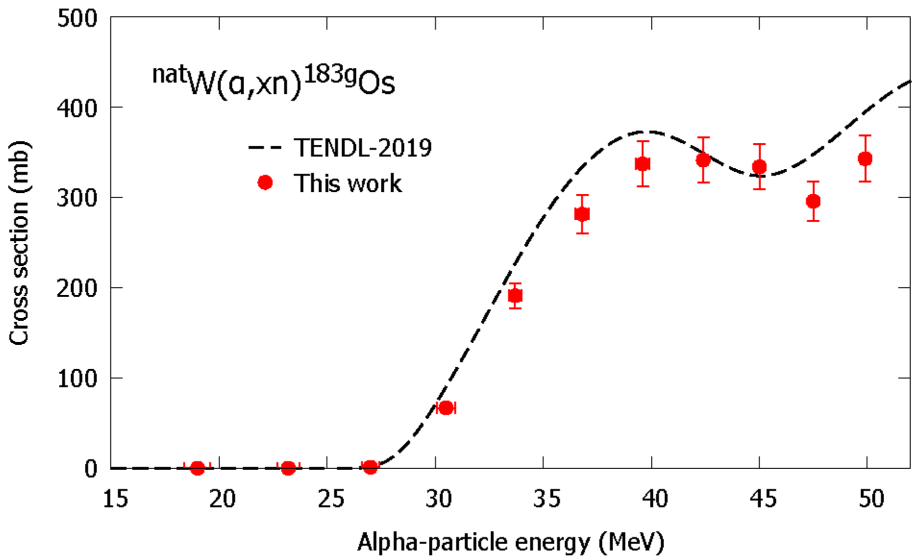

Fig. 4. Cross sections of the $^{nat}W(\alpha,xn)^{183g}Os$ reaction with the TENDL-2019 values [17].

3.4 The $^{nat}W(\alpha,xn)^{182g}Os$ reaction

Osmium-182 has the short-lived metastable state ^{182m}Os at 1.8 MeV ($T_{1/2}$ = 0.78 ms) that decayed soon after the end-of-bombardment. Cumulative cross sections for the ^{182g}Os ($T_{1/2}$ = 21.84 h) production were determined using the spectra in Ser. 1. The intense gamma lines at 180.20 keV (I_γ = 34.1%) and 263.29 keV (I_γ = 6.76%) were not selected because of several possible interfering gamma lines from ^{183}Os, ^{182m}Re, and ^{182g}Re. The gamma line at 130.80 keV (I_γ = 3.30%) was instead selected. The gamma line included contribution of the gamma line at 130.81 keV (I_γ = 7.5%) from ^{182g}Re. The contribution was estimated using more intense gamma line at 1427.3 keV (I_γ = 9.8%) and found to be negligibly small. The self-absorption of the gamma line was calculated using Eq. (1) and the mass attenuation coefficient [14]. The estimated absorption was 4.1%. The corrected counts were used to derive the cross sections.

The derived cross sections are shown in Fig. 5 in comparison with theoretical prediction of TENDL-2019 and TENDL-2021 [17]. The TENDL-2019 and TENDL-2021 data are slightly deviated from our data. According to the TENDL data, the dominant reaction below 50 MeV is the $^{182}W(\alpha,4n)^{182g}Os$ reaction. There are no experimental data found in the literature survey.

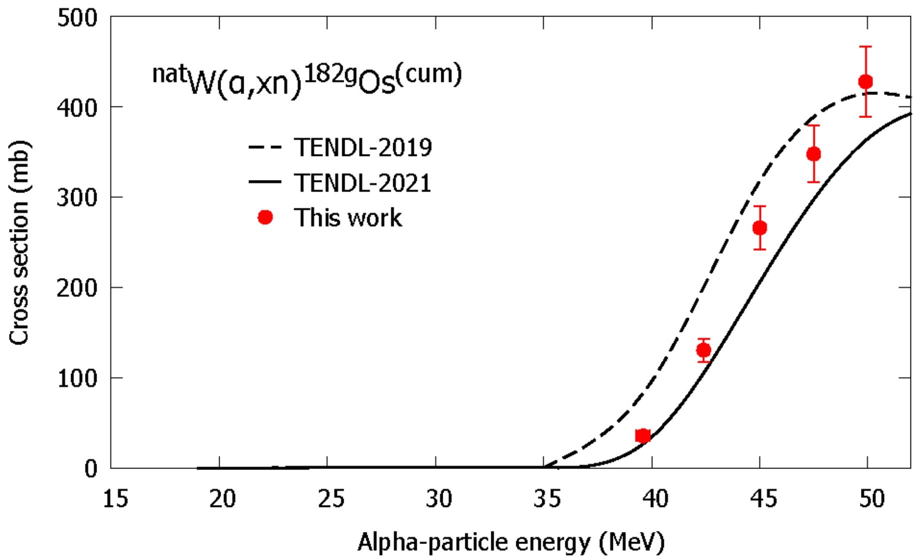

Fig. 5. Cumulative cross sections of the $^{nat}W(\alpha,xn)^{182g}Os$ reaction with the TENDL-2019 and TENDL-2021 values [17].

3.5 The $^{nat}W(\alpha,x)^{188g}Re$ reaction

The production cross sections of ^{188g}Re ($T_{1/2}$ = 17.003 h) were determined using the spectra in Ser. 1. The short-lived metastable state ^{188m}Re ($T_{1/2}$ = 18.59 min) decayed to ^{188g}Re during cooling time. No peaks of the parent nucleus ^{188}W ($T_{1/2}$ = 69.78 d) were found in any spectra and its contribution was neglected. The intense gamma line at 155.044 keV (I_γ = 15.49%) was used to determine the cross sections. The gamma line was interfered by 154.10 (I_γ = 0.23%) and 156.39 keV (I_γ = 7.2%) from ^{182g}Re, 156.38 keV (I_γ = 0.54%) from ^{182m}Re and 154.4 keV (I_γ = 0.27%) from ^{181}Re. The contribution of the interference could not be well estimated nor subtracted. Only two points below 30.5 MeV could be determined because no peaks of ^{182g}Re, ^{182m}Re and ^{181}Re were found in the corresponding foils and their contribution was expected to be negligible. The self-absorption of the low energy gamma line was calculated using Eq. (1) and the mass attenuation coefficient of 1.50 cm^2/g, which was interpolated from the values in the online database [14]. The self-absorption in the ^{nat}W foil was estimated as 2.3%. The cross sections were derived using the counts of the gamma line corrected by that factor.

The derived cross sections are shown in Fig. 6 with the experimental data in the literature [6,7] and the theoretical prediction of TENDL-2019 and TENDL-2021 [17]. The literature data measured on ^{186}W enriched targets were normalized to those using natural targets taking into account the abundance of ^{186}W in natural tungsten. In addition, the cross section of Scott et al. (1968) was multiplied by 0.61 to adjust difference of the gamma-ray intensity between their adopted (I_γ = 9.5%) and recent values (I_γ = 15.49%). The normalized data of Scott et al. (1968) are larger than the other experimental data. The data of Aliev et al. (2021) are consistent with ours. Both datasets of TENDL are lower than the experimental data below 30.5 MeV. The TENDL-2021 values agree with the data of Aliev et al. (2021), though only a partial agreement with the TENDL-2019 values is seen around 40 MeV.

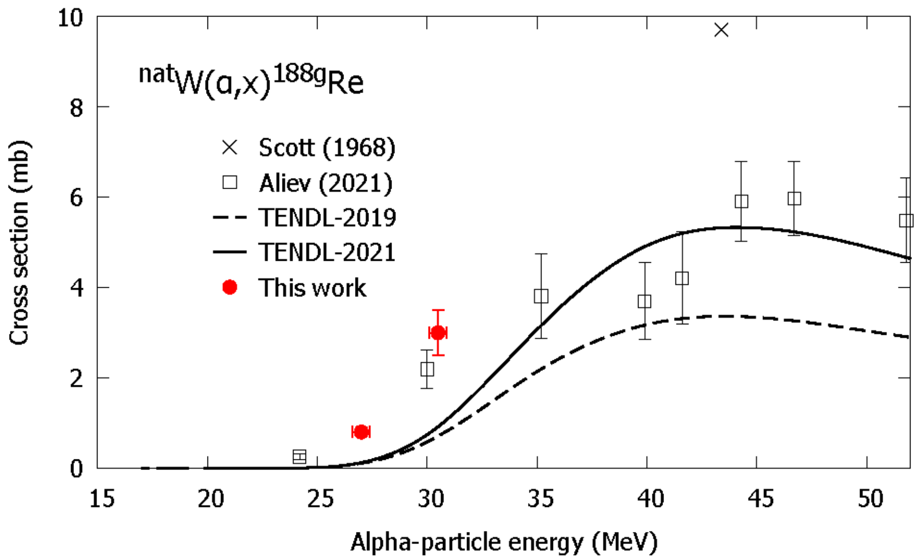

Fig. 6. Cumulative cross sections of the $^{nat}W(\alpha,x)^{188g}Re$ reaction with the literature data [6,7] normalized to natural tungsten targets and the TENDL-2019 and TENDL-2021 values [17].

3.6 The $^{nat}W(\alpha,x)^{186g}Re$ reaction

Rhenium-186 has two metastable states, the shorter-lived ground state ^{186g}Re ($T_{1/2}$ = 3.7183 d) and the longer-lived excited state ^{186m}Re ($T_{1/2}$ = 2.0×10^5 y). The excited state ^{186m}Re could be produced simultaneously but the contribution of the decay to ^{186g}Re was negligible because of the long half-life. The gamma line at 137.157 keV (I_γ = 9.47%) observed in the spectra in Ser. 3 was used to derive the production cross sections of ^{186g}Re. The possible interference of 137.2 keV (I_γ = 0.07%) from ^{181}Re ($T_{1/2}$ = 19.9 h) was negligibly small because of the very low gamma-ray intensity. The self-absorption of the 137.157-keV gamma line was estimated as 3.5% and the net counts were corrected accordingly.

The derived cross sections are shown in Fig. 7 with the theoretical prediction of TENDL-2019 [17]. The TENDL-2019 data have slightly different tendency from our data but they have similar amplitude. There are no experimental data found in the literature survey.

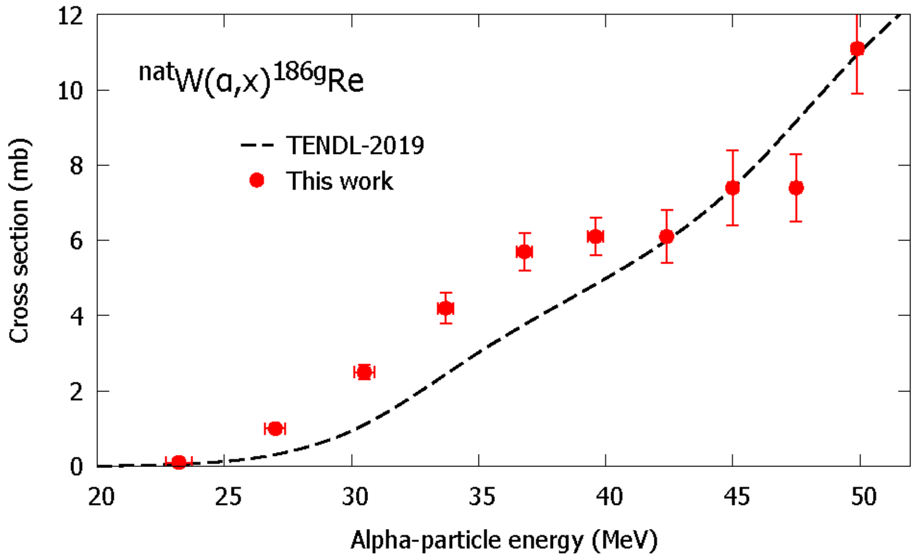

Fig. 7. Cross sections of the $^{nat}W(\alpha,x)^{186g}Re$ reaction with the TENDL-2019 values [17].

3.7 The $^{nat}W(\alpha,x)^{184g}Re$ reaction

The production cross sections of ^{184g}Re ($T_{1/2}$ = 35.4 d) were determined using the gamma line at 903.282 keV (I_γ = 38.1%) observed in the spectra in Ser. 3. The metastable state ^{184m}Re ($T_{1/2}$ = 169 d) partially decayed to ^{184g}Re by internal transition (IT: 74.5%) and to ^{184}W by $\varepsilon+\beta^+$ decay ($\varepsilon+\beta^+$: 25.5%) during the cooling time. Both the decay contribution of the ^{184m}Re to ^{184g}Re and the interference of the same gamma line at 903.282 keV (I_γ = 3.74%) from ^{184m}Re were neglected because the more intense gamma line at 104.7395 keV (I_γ = 13.6%) from ^{184m}Re could not be found in any spectra. The 903.282-keV gamma rays emitted with decay of ^{184}Ta ($T_{1/2}$ = 8.7 h) was also neglected due to the applied cooling time (3.0-4.8 d).

The derived cross sections are shown in Fig. 8 with the theoretical prediction of TENDL-2019 [17]. The TENDL-2019 prediction consisting of the reactions on three isotopes (^{182}W, ^{183}W and ^{184}W) is lower than our data. There are no experimental data found in the literature survey.

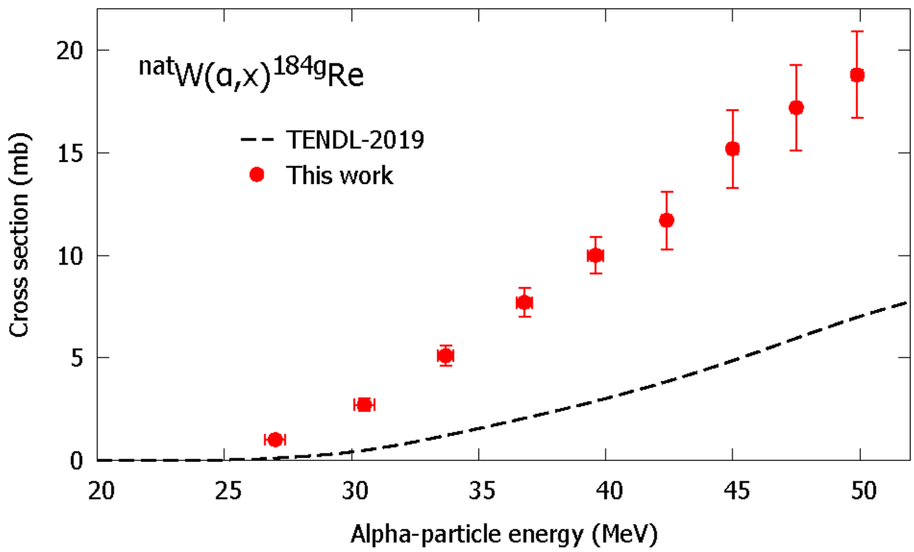

Fig. 8. Cross sections of the $^{nat}W(\alpha,x)^{184g}Re$ reaction with the TENDL-2019 values [17].

3.8 The $^{nat}W(\alpha,x)^{183g}Re$ reaction

Rhenium-183 has three short-lived excited states ($T_{1/2}$ = 7.8 ns, 1.04 ms, and 10 ns) and the three states decay to the longer-lived ground state ^{183g}Re ($T_{1/2}$ = 70.0 d). Production cross sections of ^{183g}Re were measured using the spectra in Ser. 3. More than 98% of the co-produced parents ^{183g}Os ($T_{1/2}$ = 13.0 h) and ^{183m}Os ($T_{1/2}$ = 9.9 h) were expected to decay during the cooling time. The gamma line at 162.33 keV (I_γ = 25.1%) was used for cross section deduction. The contribution of the 162.852-keV gamma line (I_γ = 0.57%) from ^{185}Os ($T_{1/2}$ = 93.6 d) was estimated using the more intense gamma line at 646.116 keV (I_γ = 78%) and was subtracted. The self-absorption of the 162.33-keV gamma line was 2.1% and the corrected counts were used for the cross sections.

The cumulative cross sections are shown in Fig. 9 with the theoretical prediction of TENDL-2019 and TENDL-2021 [17]. The contribution through the decay of ^{183g}Os and ^{183m}Os is dominant. Both TENDL datasets are consistent with our data although the shapes of the two calculations are slightly different. There are no experimental data found in the literature survey.

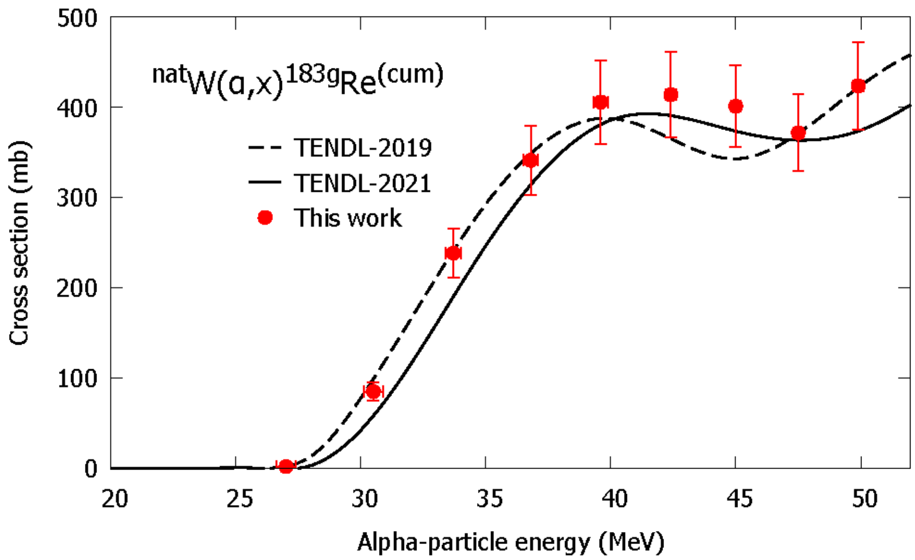

Fig. 9. Cumulative cross sections of the $^{nat}W(\alpha,x)^{183g}Re$ reaction with the TENDL-2019 and TENDL-2021 values [17].

3.9 The $^{nat}W(\alpha,x)^{182g}Re$ reaction

The ^{182}Re has two isomeric states, the ground state and the higher laying excited state. The excited state has no IT decay mode to the ground state. Both of them decay directly to ^{182}W and most of the gamma lines are common. Therefore, most of the intense gamma lines of ^{182g}Re ($T_{1/2}$ = 64.2 h) are in interference with those from decay of its excited state ^{182m}Re ($T_{1/2}$ = 14.14 h). The interference-free gamma line at 1427.3 keV (I_γ = 9.8%) of the spectra in Ser. 3 was selected to determine production cross sections of ^{182g}Re. The parent ^{182g}Os ($T_{1/2}$ = 21.84 h) decays only to ^{182m}Re ($T_{1/2}$ = 14.14 h), and ^{182m}Re decays to ^{182}W. The sequential decay was expected to have no contribution to ^{182g}Re production. The decay curve analysis using spectra of the three measurement series supported the negligible contribution.

The derived cross sections are shown in Fig. 10 with the theoretical prediction of TENDL-2019 [17]. The dominant contributing reaction is the $^{182}W(\alpha,x)^{182g}Re$ reaction. The $^{180}W(\alpha,x)^{182g}Re$ reaction with the lower threshold energy less occurs because of the tiny isotopic ratio of ^{180}W (0.12%). The TENDL-2019 data are consistent with our data. There are no experimental data found in the literature survey.

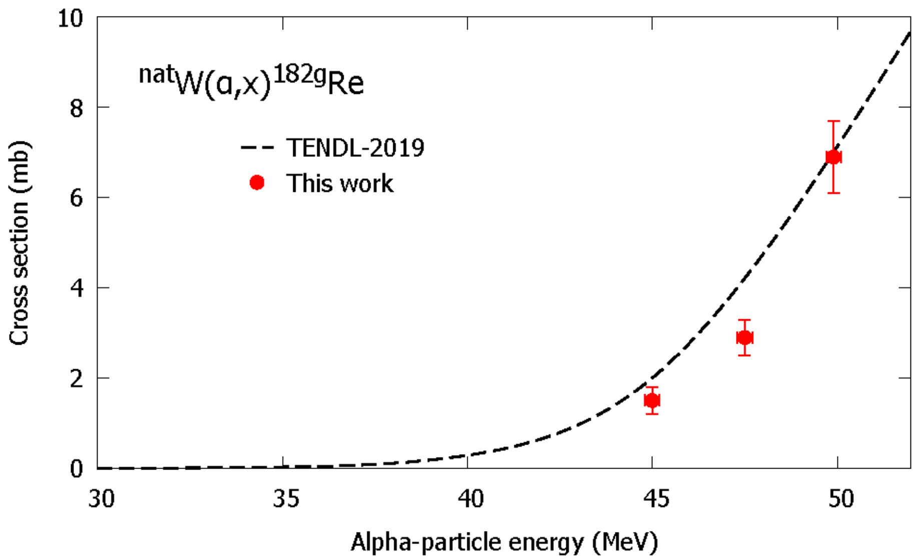

Fig. 10. Cross sections of the $^{nat}W(\alpha,x)^{182g}Re$ reaction with the TENDL-2019 values [17].

3.10 The $^{nat}W(\alpha,x)^{181}Re$ reaction

The production cross sections of ^{181}Re ($T_{1/2}$ = 19.9 h) were measured using the spectra in Ser. 1. The shorter-lived parents ^{181m}Os ($T_{1/2}$ = 2.7 min) and ^{181g}Os ($T_{1/2}$ = 105 min) decayed to ^{181}Re during the cooling time. The intense gamma line at 365.5 keV (I_γ = 56%) was used to derive the cross sections.

The cumulative cross sections are shown in Fig. 11 with the theoretical prediction of TENDL-2019 and TENDL-2012 [17]. The contribution through the decay of ^{181}Os is dominant. The TENDL-2021 values agree with our result although the TENDL-2019 data are largely deviated above 45 MeV. There are no experimental data found in the literature survey.

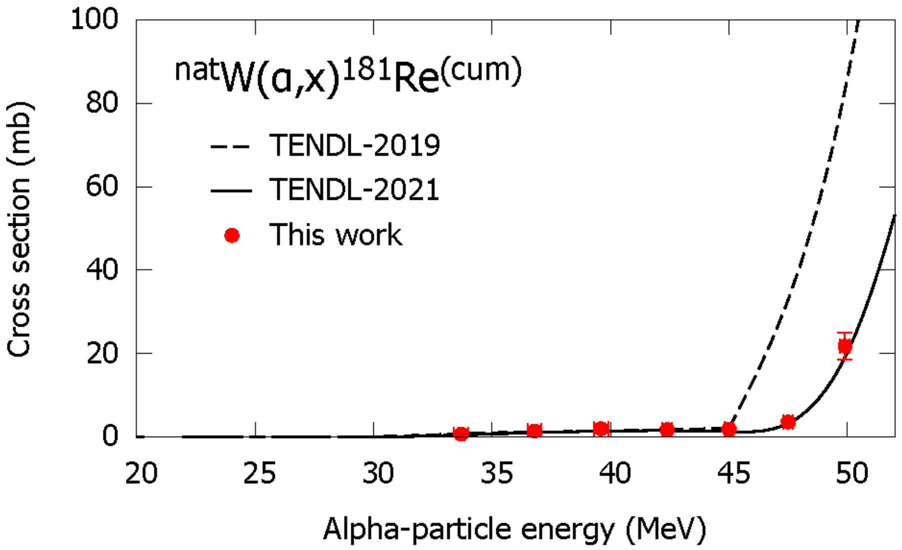

Fig. 11. Cumulative cross sections of the $^{nat}W(\alpha,x)^{181}Re$ reaction with the TENDL-2019 and TENDL-2021 values [17].

4. Conclusion

Activation cross sections of alpha-particle-induced reactions on natural tungsten were measured up to 50 MeV. The experiment was conducted at the RIKEN AVF cyclotron. The stacked-foil activation technique and gamma-ray spectrometry were used. Production cross sections of ^{185,183m,183g,182g}Os and ^{188g,186g,184g,183g,182g,181}Re were determined. The cross sections were compared with the literature data and theoretical model calculations in the TENDL-2019 and TENDL-2021 library. One of the two previous experimental studies agrees with our results. The theoretical predictions well agree with the experimental data in the most of the reactions except for the ^{nat}W(α,x)^{183m}Os and ^{nat}W(α,x)^{184g}Re reactions. Many by-products other than ^{188g,186g}Re can be produced simultaneously because of five isotopes in natural tungsten. The usage of isotopically enriched targets can avoid or reduce the production of such impurities. However, the measured production cross sections of ^{188g,186g}Re are small and the reactions may not be appropriate for practical use in medicine.

The cross sections of the most reactions are reported here for the first time. The results are expected to contribute to determine the optimal production of the radioisotopes and improvement of nuclear reaction codes.

Acknowledgment

This work was carried out at RI Beam Factory operated by RIKEN Nishina Center and CNS, University of Tokyo, Japan. The participation of the Hungarian researchers was partly supported by Project no. NKTA-42, which has been implemented with the support provided by the Ministry of Innovation and Technology of Hungary from the National Research, Development and Innovation Fund, financed under the TKP2021 funding scheme.

Declarations of interest

None.

Reference

[1] A.M. Denis-Bacelar, S.J. Chittenden, D.P. Dearnaley, A. Divoli, J.M. O'Sullivan, V.R. McCready, B. Johnson, Y. Du, G.D. Flux, Phase I/II trials of ^{186}Re-HEDP in metastatic castration-resistant prostate cancer: post-hoc analysis of the impact of administered activity and dosimetry on survival, Eur. J. Nucl. Med. Mol. Imaging. 44 (2017) 620–629. https://doi.org/10.1007/s00259-016-3543-x.

[2] I.G. Finlay, M.D. Mason, M. Shelley, Radioisotopes for the palliation of metastatic bone cancer: a systematic review, Lancet Oncol. 6 (2005) 392–400. https://doi.org/10.1016/S1470-2045(05)70206-0.

[3] M. Argyrou, A. Valassi, M. Andreou, M. Lyra, Rhenium-188 Production in Hospitals, by W-188/Re-188 Generator, for Easy Use in Radionuclide Therapy, Int. J. Mol. Imaging. 2013 (2013) 1–7. https://doi.org/10.1155/2013/290750.

[4] N. Otuka, E. Dupont, V. Semkova, B. Pritychenko, A.I. Blokhin, M. Aikawa, S. Babykina, M. Bossant,

G. Chen, S. Dunaeva, R.A. Forrest, T. Fukahori, N. Furutachi, S. Ganesan, Z. Ge, O.O. Gritzay, M. Herman, S. Hlavač, K. Kato, B. Lalremruata, Y.O. Lee, A. Makinaga, K. Matsumoto, M. Mikhaylyukova, G. Pikulina, V.G. Pronyaev, A. Saxena, O. Schwerer, S.P. Simakov, N. Soppera, R. Suzuki, S. Takács, X. Tao, S. Taova, F. Tárkányi, V. V. Varlamov, J. Wang, S.C. Yang, V. Zerkin, Y. Zhuang, Towards a More complete and accurate experimental nuclear reaction data library (EXFOR): International collaboration between nuclear reaction data centres (NRDC), Nucl. Data Sheets. 120 (2014) 272–276. https://doi.org/10.1016/j.nds.2014.07.065.

[5] B. Pritychenko, E. Běták, M.A. Kellett, B. Singh, J. Totans, The Nuclear Science References (NSR) database and Web Retrieval System, Nucl. Instruments Methods Phys. Res. Sect. A Accel. Spectrometers, Detect. Assoc. Equip. 640 (2011) 213–218. https://doi.org/10.1016/j.nima.2011.03.018.

[6] N.E. Scott, J.W. Cobble, P.J. Daly, A comparison of reactions induced by medium-energy ^{3}He and ^{4}He ions in heavy target nuclei, Nucl. Phys. A. 119 (1968) 131–145. https://doi.org/10.1016/0375-9474(68)90810-5.

[7] R.A. Aliev, V.A. Zagryadskiy, E.S. Kormazeva, S.T. Latushkin, T.Y. Malamut, A.N. Moiseeva, V.I. Novikov, I.I. Skobelin, V.N. Unezhev, Measurement of ^{186}W(^{4}He, p3n)^{186}Re, ^{186}W(^{4}He, pn)^{188}Re, ^{186}W(^{4}He, p)^{189}Re reaction cross sections by ^{4}He irradiation of ^{186}W target, At. Energy. 130 (2021) 36–39. https://doi.org/10.1007/s10512-021-00770-3.

[8] J. Meija, T.B. Coplen, M. Berglund, W.A. Brand, P. De Bièvre, M. Gröning, N.E. Holden, J. Irrgeher, R.D. Loss, T. Walczyk, T. Prohaska, Isotopic compositions of the elements 2013 (IUPAC Technical Report), Pure Appl. Chem. 88 (2016) 293–306. https://doi.org/10.1515/pac-2015-0503.

[9] National Nuclear Data Center, Nuclear structure and decay data on-line library, Nudat 3.0, (2021). http://www.nndc.bnl.gov/nudat3/.

[10] International Atomic Energy Agency, LiveChart of Nuclides, (2009). https://www-nds.iaea.org/livechart/.

[11] S.Y.F. Chu, L.P. Ekström, R.B. Firestone, The Lund/LBNL Nuclear Data Search, (1999). http://nucleardata.nuclear.lu.se/toi/.

[12] B. Pritychenko, A. Sonzogni, Q-value Calculator (QCalc), (2003). http://www.nndc.bnl.gov/qcalc/.

[13] Z.B. Alfassi, E. Persico, F. Groppi, M.L. Bonardi, On the photon self-absorption correction for thin-target-yields vs. thick-target-yields in radionuclide production, Appl. Radiat. Isot. 67 (2009) 240–242. https://doi.org/10.1016/j.apradiso.2008.10.004.

[14] J.H. Hubbel, S.M. Seltzer, X-Ray Mass Extinction Coefficients, NIST Stand. Ref. Database 126. (2004). https://doi.org/https://doi.org/10.18434/T4D01F.

[15] A. Hermanne, A. V. Ignatyuk, R. Capote, B. V. Carlson, J.W. Engle, M.A. Kellett, T. Kibédi, G. Kim, F.G. Kondev, M. Hussain, O. Lebeda, A. Luca, Y. Nagai, H. Naik, A.L. Nichols, F.M. Nortier, S. V. Suryanarayana, S. Takács, F.T. Tárkányi, M. Verpelli, Reference Cross Sections for Charged-particle Monitor Reactions, Nucl. Data Sheets. 148 (2018) 338–382. https://doi.org/10.1016/j.nds.2018.02.009.

[16] F. Tárkányi, S. Takács, K. Gul, A. Hermanne, M.G. Mustafa, M. Nortier, P. Obložinský, S.M. Qaim, B.

Scholten, Y.N. Shubin, Z. Yousiang, Beam monitor reactions, in: Charg. Part. Cross-Section Database Med. Radioisot. Prod. IAEA-TECDOC-1211, 2001.

[17] A.J. Koning, D. Rochman, J. Sublet, N. Dzysiuk, M. Fleming, S. van der Marck, TENDL: Complete Nuclear Data Library for Innovative Nuclear Science and Technology, Nucl. Data Sheets. 155 (2019) 1–55. https://doi.org/10.1016/j.nds.2019.01.002.